Three candidate double clusters in the LMC: truth or dare?

Emanuele Dalessandro,[1][*] Alice Zocchi,[1,2] Anna Lisa Varri,[3] Alessio Mucciarelli,[1,2] Michele Bellazzini,[1] Francesco R. Ferraro,[1,2] Barbara Lanzoni, [1,2] Emilio Lapenna, [1,2] and Livia Origlia [1]

[1] *INAF - Osservatorio Astronomico di Bologna, via Gobetti 93/3, I-40129, Bologna, Italy*
[2] *Dipartimento di Fisica & Astronomia, Universitá degli Studi di Bologna, via Gobetti 93/2, I-40129, Bologna, Italy*
[3] *Institute for Astronomy, University of Edinburgh, Royal Observatory, Blackford Hill, Edinburgh EH9 3HJ, UK*

ABSTRACT

The Large Magellanic Cloud (LMC) hosts a large number of candidate stellar cluster pairs. Binary stellar clusters provide important clues about cluster formation processes and the evolutionary history of the host galaxy. However, to properly extract and interpret this information, it is crucial to fully constrain the fraction of real binary systems and their physical properties. Here we present a detailed photometric analysis based on ESO-FORS2 images of three candidate cluster multiplets in the LMC, namely SL349-SL353, SL385-SL387-NGC1922 and NGC1836-BRHT4b-NGC1839. For each cluster we derived ages, structural parameters and morphological properties. We have also estimated the degree of filling of their Roche lobe, as an approximate tool to measure the strength of the tidal perturbations induced by the LMC. We find that the members of the possible pairs SL349-SL353 and BRHT4b-NGC1839 have a similar age ($t = 1.00 \pm 0.12$ Gyr and $t = 140 \pm 15$ Myr, respectively), thus possibly hinting to a common origin of their member systems We also find that all candidate pairs in our sample show evidence of intra-cluster overdensities that can be a possible indication of real binarity. Particularly interesting is the case of SL349-SL353. In fact, SL353 is relatively close to the condition of critical filling, thus suggesting that these systems might actually constitute an energetically bound pair. It is therefore key to pursue a detailed kinematic screening of such clusters, without which, at present, we do not dare making a conclusive statement about the true nature of this putative pair.

Key words: galaxies: star clusters: general - Magellanic Clouds - techniques: photometric - globular clusters: general

1 INTRODUCTION

It is commonly accepted that star clusters form from the fragmentation of giant molecular clouds in cloud cores that eventually produce stellar complexes, OB association or larger systems (Efremov 1995). However, the exact mechanisms of formation are not understood yet and likely there are different paths that lead to the formation of different systems of clusters. Particularly intriguing is the idea that star clusters could form in pairs or multiplets (de La Fuente Marcos & de La Fuente Marcos 2009).

Indeed, both the Milky Way (MW) and the Large Magellanic Cloud (LMC) stellar cluster systems contain a sizable

population ($\sim 10\%$) of massive and young/intermediate age clusters, with projected mutual distance ≤ 20 pc (Bhatia & Hatzidimitriou 1988; Bhatia et al. 1991; Surdin 1991; Subramaniam et al. 1995; Dieball et al. 2002; Mucciarelli et al. 2012; De Silva et al. 2015). On the other hand, in both systems double old clusters are completely lacking. Statistical arguments indicate that the LMC binary cluster population cannot be simply explained in terms of projection effects, but gravitationally bound systems should be a relevant fraction of the listed candidates (Bhatia & Hatzidimitriou 1988; Dieball et al. 2002). An additional handful of binary clusters are also known in the nearby Universe, in the Small Magellanic Cloud (SMC; Hatzidimitriou & Bhatia 1990), in M31 (Holland et al. 1995), in NGC5128 (Minniti et al. 2004), in

the Antennae galaxies (Fall et al. 2005) and in the young starburst galaxy M51 (Larsen 2000).

There are three possible explanations for the origin of these systems: (1) they formed from the fragmentation of the same molecular cloud (Elmegreen & Elmegreen 1983), (2) they were generated in distinct molecular clouds and then became bound systems after a close encounter leading to a tidal capture (Vallenari et al. 1998; Leon et al. 1999), or (3) they are the result of division of a single star-forming region (Goodwin & Whitworth 2004; Arnold et al. 2017). Their subsequent evolution may also have different outcomes. Dynamical models and N-body simulations (see, e.g. Barnes & Hut 1986; de Oliveira et al. 1998, and references therein) have shown that, depending on the initial conditions, a bound pair of clusters may either become unbound, because of significant mass loss in the early phases of stellar evolution, or merge into a single and more massive cluster on a short timescale (≈ 60 Myr) due to loss of angular momentum from escaping stars (see Portegies Zwart & Rusli 2007). The final product of a merger may be characterized by a variable degree of kinematic and morphologic complexity, mostly depending on the values of the impact parameter of the pre-merger binary system (de Oliveira et al. 2000; Priyatikanto et al. 2016). In some cases, the stellar system resulting from the merger event may show significant internal rotation (in fact, for many years this has been the preferred dynamical route to form rotating star clusters, see Sugimoto & Makino 1989; Makino et al. 1991; Okumura et al. 1991; de Oliveira et al. 1998). Merger of cluster pairs has been sometimes invoked to interpret the properties of particularly massive and dynamically complex clusters (e.g., see the study of ω Centauri by Lee et al. 1999, G1 by Baumgardt et al. 2003, and NGC2419 by Brüns & Kroupa 2011), and, more in general, as an avenue to form clusters with multiple populations with different chemical abundances both in terms of iron and light-elements (e.g., van den Bergh 1996; Catelan 1997; Amaro-Seoane et al. 2013; Gavagnin et al. 2016; Hong et al. 2017).

The population and the properties of binary clusters could depend on the past evolutionary history of the host galaxy. In fact, several theoretical investigations suggest that encounters and interactions between the LMC and the SMC triggered the formation of binary systems and, on a larger extent, the formation of most of the known GCs in the LMC/SMC system. For example, Kumai et al. (1993) pointed out that, if interstellar gas clouds have large-scale random motions in the interacting LMC/SMC system, then they may collide to form compact star clusters through strong shock compression. Bekki et al. (2004) demonstrated that the star formation efficiency in interacting galaxies can significantly increase, resulting in the formation of compact stellar systems and double clusters. This idea is supported by the link between the two bursts of cluster formation in the LMC (~ 100 Myr and $1-2$ Gyr ago; Girardi et al. 1995) and the epochs of the closest encounters between the SMC and LMC, as predicted by various theoretical models (Gardiner & Noguchi 1996; see also Kallivayalil et al. 2013, for more recent models and references).

In principle, then, the study of cluster pairs provides crucial information about the mechanisms of cluster formation and evolution, and the possible interactions suffered by
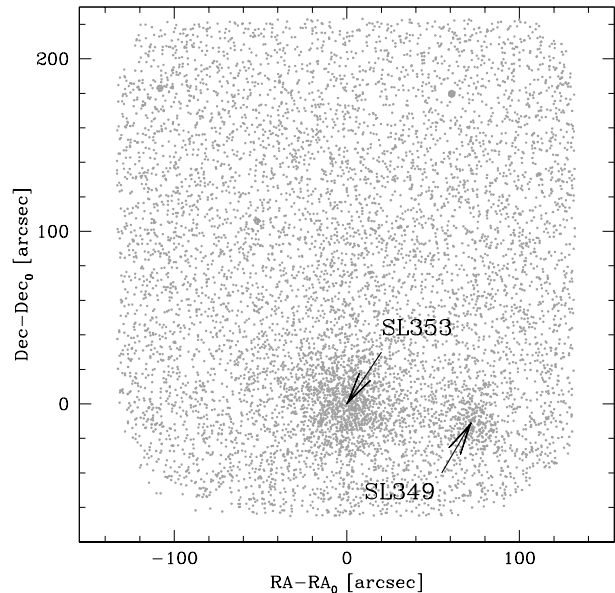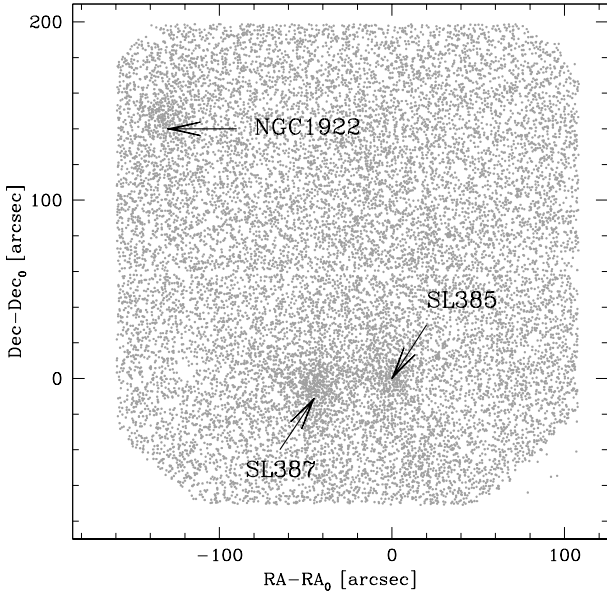

Figure 1. Map of the candidate cluster pair SL349-SL353 obtained with FORS2. The centre of each cluster is indicated with an arrow.

the host galaxy in the past. In practice, however, very little is known to date about these systems.

Up to now the criterion typically used to select cluster pairs has been the observed small angular separation ($d < 1.4'$; Dieball et al. 2002) and the only additional hint is the evidence that in some of these candidates the two components appear to be coeval. However, age estimates are quite uncertain, since they are usually derived exclusively from integrated colors (e.g., Bica et al. 1996), as rich color-magnitude diagrams (CMDs; e.g. Vallenari et al. 1998) are avaialble only in a few cases. So far, the binarity has been confirmed by means of a detailed chemical analysis and radial velocities obtained with high-resolution spectra only in the case of NGC2136 - NGC2137 in the LMC (Mucciarelli et al. 2012) and NGC5617 - Trumpler22 in the Galaxy (De Silva et al. 2015).

In this work we attempt to provide a more robust characterization of three candidate cluster pairs in the LMC: SL349-SL353, SL387-SL385 and NGC1836-BRHT4b. We use three main quantities to assess their nature (i.e. possible binarity): 1) ages from Main-Sequence Turn-OFF (MSTO) luminosity in well populated CMDs; 2) cluster structure parameters as derived by number counts of resolved stars; 3) evidence of tidal distortions and analysis of possible signatures of interaction with their tidal environment.

The manuscript is organized as follows: Section 2 provides a description of the images obtained with FORS2 at the Very Large Telescope and their corresponding analysis. An age estimate of the star clusters under consideration is presented in Section 3. The structural and dynamical properties of the clusters are discussed in Section 4, in Section 5 we analyze tidal effects on the stellar systems. Finally, we discuss our results and present our conclusions in Section 6.

Figure 2. Map of the candidate cluster pair SL387-SL385; the stellar system NGC 1922 is also visible within the field of view. The centre of each cluster is indicated with an arrow.
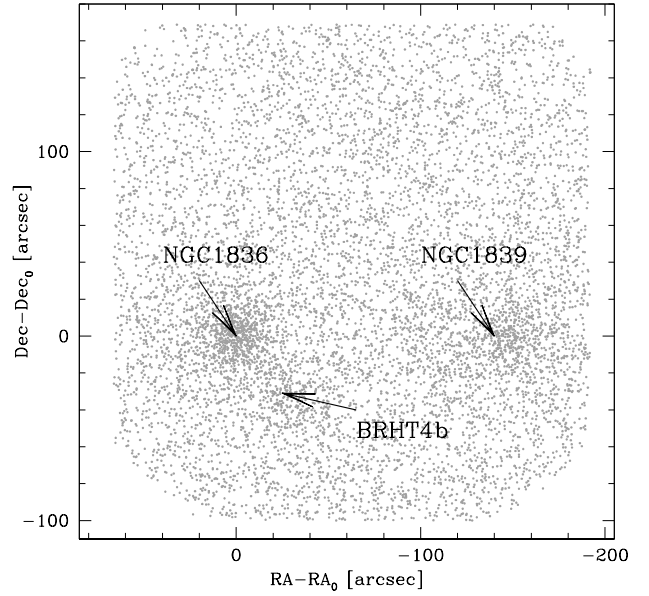
Figure 3. Map of the candidate cluster pair NGC1836-BRHT4b; the stellar system NGC1839 is also visible within the field of view. The centre of each cluster is indicated with an arrow.

2 OBSERVATIONS AND DATA ANALYSIS

The data-set used in this paper consists of a combination of $V_{\rm HIGH}$ and $I_{\rm BESSEL}$ images obtained with the wide-field imager FORS2 at the Very Large Telescope (Prop ID: 090.D-0348, PI: Mucciarelli). Observations were obtained by using the $2k \times 4k$ pixels MIT Red-optimized CCD mosaic in the high-resolution mode ($\sim 0.12''$ pixel^{-1}), which yields a total field of view (FOV) of about $3.4' \times 3.4'$. In all cases, candidate cluster pairs were centered in chip#1 (Figures 1-3). In the FORS2 images targeting SL385-SL387 and NGC1836-BRHT4b we also observe NGC1922 and NGC1839 respectively (see Figures. 2, 3). The projected distances of these two clusters from the candidate cluster pairs is larger than $120''$. According to Bhatia (1990) and Sugimoto & Makino (1989), binary clusters with such large separations may become detached by external tidal forces in relatively short timescales. As a consequence we will consider them as unbound from the nearby candidate pairs. However, they will be included in the following analysis.

For SL349-SL353, 16 images have been obtained both for $V_{\rm HIGH}$ and $I_{\rm BESSEL}$ with a combination of 10 long exposures ($t_{\rm exp} = 240$s and $t_{\rm exp} = 280$s for $V_{\rm HIGH}$ and $I_{\rm BESSEL}$ respectively) and six images for each band with $t_{\rm exp} = 10$s. 17 images have been acquired in $I_{\rm BESSEL}$ band and 16 in the $V_{\rm HIGH}$ for SL385-SL387: 10×240s $+ 7 \times 10$s in $I_{\rm BESSEL}$ and 10×280s $+ 6 \times 10$s in $V_{\rm HIGH}$. In the case of NGC1836-BRHT4b a total of 15 images have been acquired in the $V_{\rm HIGH}$ band, 10 with exposure time $t_{\rm exp} = 100$s and five with $t_{\rm exp} = 10$s, and a total of 15 images in the $I_{\rm BESSEL}$ with the same combination of short and long exposures. A dither pattern of $\sim 25''$ has been adopted for all targets to allow for a better reconstruction of the point-spread function (PSF) and to avoid CCD blemishes and artifacts. Master

bias and flat-fields have been reconstructed by using a large number (> 20) of calibration frames. Then scientific images have been corrected for bias and flat-field by using standard procedures and tasks contained in the Image Reduction and Analysis Facility (IRAF).[1]

Following the same approach as in Dalessandro et al. (2015a), the photometric analysis has been performed independently for each image and chip by using DAOPHOT IV (Stetson 1987). For each frame we selected several tens of bright, not saturated, and relatively isolated stars to model the PSF. For each chip the best PSF model was then applied to all sources at 3σ above the background by using DAOPHOT/ALLSTAR. We then created a master list of stars composed by sources detected at least in four frames. In each single frame, at the corresponding positions of the stars present in the master list, a fit was forced with DAOPHOT/ALLFRAME (Stetson 1994) For each star, different magnitude estimates in each filter were homogenized and their weighted mean and standard deviation were finally adopted as star magnitudes and photometric errors. Instrumental magnitudes were transformed to the Johnson/Cousin standard photometric system by using the stars in common with the catalog of Zaritsky et al. (2004) as secondary photometric standards. A few hundreds stars were found in the FOV of each candidate pair spanning the entire color range. Instrumental coordinates (x,y) were reported to the absolute (α, δ) system by using the stars in common with 2MASS and the cross-correlation tool CataXcorr[2].

---

[1] IRAF is written and supported by the National Optical Astronomy Observatories (NOAO), which is operated by the Association of Universities for Research in Astronomy, Inc., under a cooperative agreement with the National Science Foundation.
[2] CataXcorr is a code aimed at cross-correlating catalogs and

Table 1. Estimated ages and gravity center of the clusters, see Sections 3 and 4.1 for details

Cluster	t (Myr)	α (h:m:s)	δ (deg:$'$:$''$)
SL353	1000 ± 120	05:17:07.938	-68:52:24.51
SL349	1000 ± 120	05:16:54.524	-68:52:35.61
SL385	240 ± 15	05:19:25.241	-69:32:27.99
SL387	740^{+150}_{-120}	05:19:33.686	-69:32:32.62
NGC1922	90 ± 10	05:19:50.353	-69:30:01.04
NGC1836	400 ± 50	05:05:35.700	-68:37:42.56
NGC1839	140 ± 15	05:06:02.596	-68:37:43.13
BRHT4b	140 ± 15	05:05:40.572	-68:38:14.50

At this stage, the catalogs obtained for each chip are on the same photometric and astrometric system. They have been combined to form a single catalog for each candidate pair. Stars in common between different pointing have been used to check for the presence of residuals in the calibration procedure. The resulting color-magnitude diagrams (CMDs) are shown in Figs 4-6.

3   AGE ESTIMATES

In order to constrain the possible binarity of the candidate pairs in our sample, we will use in the following three main diagnostics (see Introduction). In this Section, we start by deriving the cluster ages. Ages of stellar systems in pairs can provide important clues about their formation. Clusters with similar ages likely formed from the same molecular cloud, while systems with significantly different ages are more likely unbound or the result of a capture event.

The ages of the clusters were derived by comparing CMDs with a set of PARSEC isochrones (Bressan et al. 2012). For all clusters we adopted a metallicity of $Z = 0.006$ ([Fe/H]~ -0.4), which is compatible with high-resolution spectroscopic estimates obtained for intermediate and young GCs in the LMC (see for example Mucciarelli et al. 2008, 2012), a true distance modulus $(m - M)_0 = 18.55$ and reddening $E(B - V) = 0.08$, which are compatible with typical values reported in the literature (see for example Inno et al. 2016 and Haschke et al. 2011).

In the following we list the results obtained for each candidate pair.

SL349 - SL353 - To minimize the impact of field star contamination, which can significantly affect the age determination, we used only stars located at distance $r < 35''$ and $r < 25''$ from the gravity centers of SL349 and SL353 respectively (see Section 4.1). The resulting CMDs are shown in Fig. 4 (left and middle panels). For comparison we also show the CMD of stars located at a distance $r > 200''$ from both clusters, which are representative of the surrounding field population. We find that the CMDs of SL349 and SL353 are best reproduced by models with ages $t = 1.00 \pm 0.12$ Gyr. Isochrones nicely reproduce the main sequence shape

finding solutions, developed by P. Montegriffo at INAF - Osservatorio Astronomico di Bologna.

as well as the MSTO and blue-loop star luminosity, which represents a stringent constraint to the overall fit. These ages are larger than what obtained by Dieball et al. (2000) who find $t = 550 \pm 110$ Myr for both systems based on very shallow CMDs that do not reach the cluster MSTOs, and by Piatti et al. (2015) who estimates $t = 500$ for SL349 by using VISTA near-IR observations. On the contrary, they are broadly compatible with results obtained by Bica et al. (1996), who classified both clusters in *category V*, i.e. in the age range 800-2000 Myr, by using UBV integrated colors.

SL385 - SL387 - NGC1922 - The age estimates for these clusters were performed by using stars at distances from the cluster centers $r < 30''$ for SL385 and SL387 and $r < 15''$ for NGC1922 (see Fig. 5). Figure 5 also shows the CMD of stars located at a distance $r > 150''$ from all clusters for comparison. The CMD of SL385 shows a group of bright stars at $V \sim 17$ mag and $(V - I) \sim 1$ mag mainly distributed in the innermost $10''$ and thus likely cluster members. In addition we note that this group of bright stars is not present in either the CMD of the neighbor clusters nor in that of the surrounding field. The position of these stars and the extension of the main sequence can be nicely fit by models with $t = 240 \pm 15$ Myr. This estimate is compatible with that obtained by Piatti et al. (2015). SL387 appears to be older than SL385. We find a best-fit age $t = 740^{+150}_{-120}$ Myr. These results are in good agreement within the errors with estimates obtained by Vallenari et al. (1998) for both systems based on resolved CMDs. On the contrary, Bica et al. (1996) classify both GCs in *category IVA*, which includes clusters with age t= $200 - 400$ Myr. The CMD of NGC1922 shows an extremely pronounced bright extension of the main sequence which suggests a very young age for this system. We find it can be well reproduced with models representing an age of about $t = 90 \pm 10$ Myr.

NGC1836 - BRHT4b - NGC1839 - For these three systems theoretical models were compared to stars located at distance $r < 30''$ from their gravity centers (Fig. 6). We also show a field CMD with stars located at a distance $r > 150''$ from the three clusters. At a first inspection of the CMDs, NGC1836 appears older than the other two clusters, which in fact show a MS extending up to $V \sim 16$. Also, the CMD of NGC1836 shows a clump of data points at $V \sim 18$ mag and $(V - I) \sim 1$ mag that is not evident in the CMDs of BRHT4b and NGC1839, a further indication of its older age. Indeed we find that NGC1836 can be fitted with an isochrone of age $t = 400 \pm 50$ Myr, while both BRHT4b and NGC1839 are compatible with $t = 140 \pm 15$ Myr. These values are larger than what was found by Bica et al. (1996) who obtained ages in the range 70-200 Myr and 30-70 Myr for NGC1836 and NGC1839 respectively. No estimates are available for BRHT4b.

We have verified that a variation of the adopted metallicity Δ[Fe/H]$\sim \pm 0.4$ dex have an impact on the derived ages of $\sim 10\%$. Ages obtained for all clusters are summarized in Table 1. Note that errors give the minimum and maximum age providing an acceptable fit to the CMD.
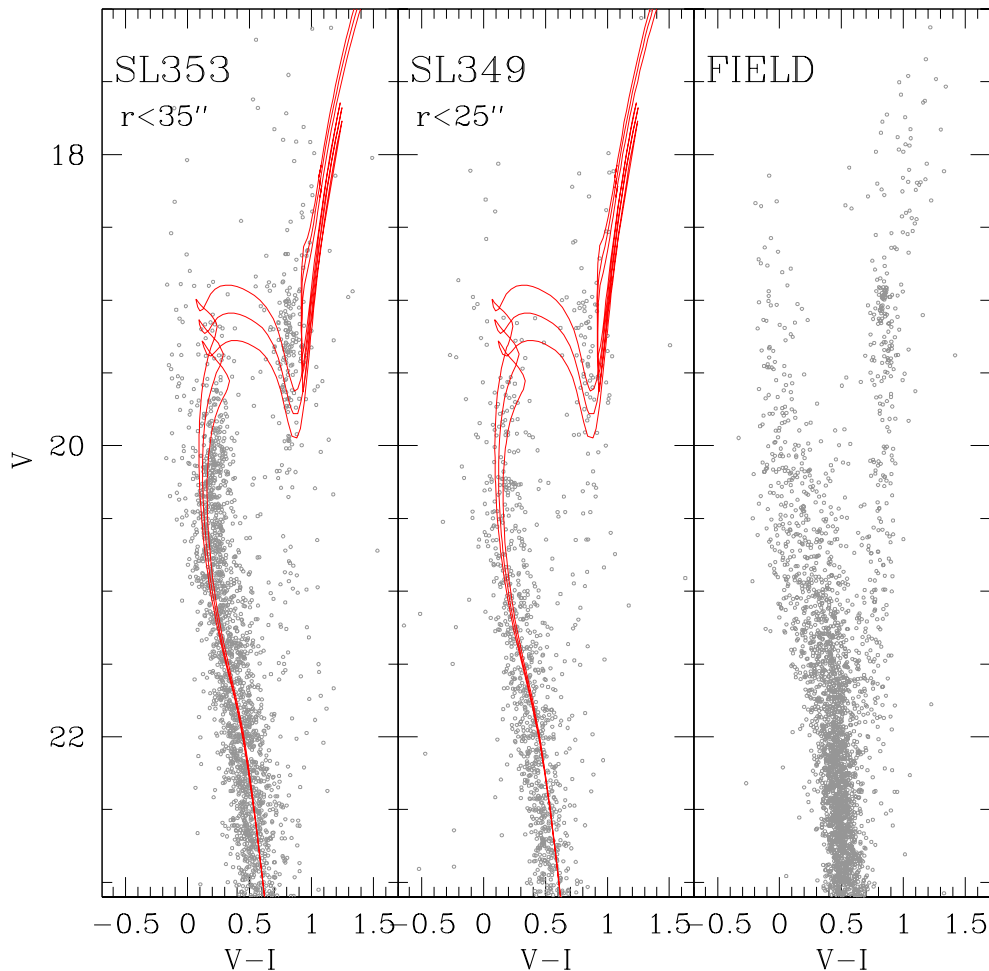
Figure 4. From left to right: color-magnitude diagrams of the clusters SL353 and SL349 and of the field stars. The area sampled by the field CMD is ~ 2.4 arcmin^2, thus more than 2.5 times the area covered by the CMDs of the two clusters. In the first two panels best-fit isochrones as well as minimun and maximum age models providing an acceptable fit are shown.

4 DENSITY PROFILES AND CLUSTER PARAMETERS

The other two diagnostics used in the present analysis to asses the binarity of the candidate pairs are mainly related to the cluster structural and morphological properties. In the following two Sections we will derive density profiles, the structural parameters of the clusters and constrain the effect of the tidal environment on their properties.

4.1 Centers of gravity and projected density profiles

As a first step to compute the cluster density profiles, we derived the center of gravity, C_{grav}, for each system by averaging the positions α and δ of properly selected stars and using an iterative procedure (see for example Lanzoni et al. 2007; Dalessandro et al. 2013). Only stars with $V \leq 21$ were used to avoid spurious effects due to incompleteness. For each target we derived centers of gravity for different radial selections typically ranging from $\sim 10''$ to $\sim 20''$ (the only

exception is SL439 for which an estimate of C_{grav} was obtained also using stars at a distance of $35''$) depending on the apparent extension of the systems and on the relative proximity to nearby clusters. We obtained a minimum of three to a maximum of five different estimates of the center for each cluster. C_{grav} was then obtained as the average of these values and the error as the standard deviation, which results to be typically of $\sim 1''$. The centers thus derived for each cluster are listed in Table 1.

The projected number density profiles were then determined by using direct star counts. Using the procedure described in Dalessandro et al. (2013), we divided the selected regions into several concentric annuli of variable width (the exact number differs from cluster to cluster depending on their extent) centered on C_{grav} and suitably split in an adequate number of sub-sectors (in the range 2-4) depending on the portion of the field of view actually sampled. In order to minimize the contamination from nearby clusters, for each stellar system in the proposed pairs we considered only subsectors located in the opposite direction to the nearest GC
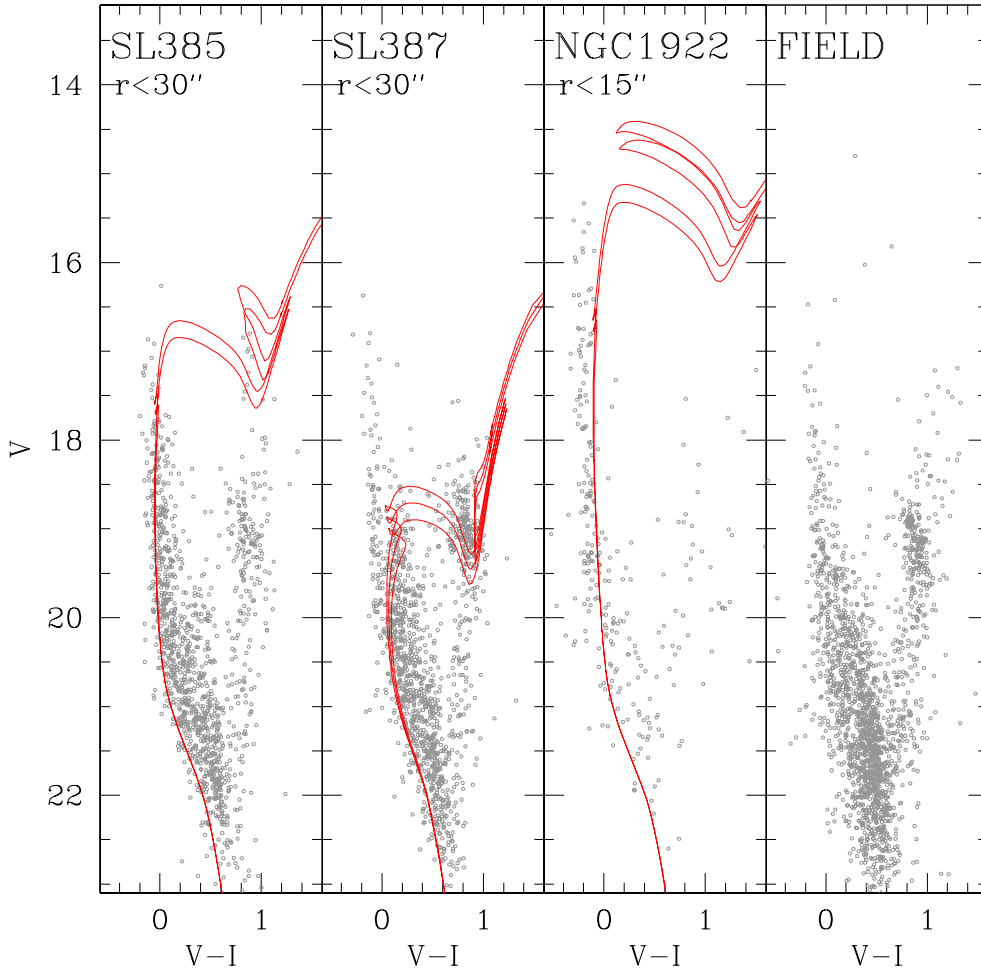
Figure 5. From left to right: color-magnitude diagrams of the clusters SL385, SL387, NGC1922, and of the field stars. The area sampled by the field CMD is ∼ 1.3arcmin². As in Figure4, best-fit isochrones and minimun/maximum age models providing an acceptable fit are shown.

(see Figs 1, 2 and 3). Number counts were calculated in each sub-sector and the corresponding densities were obtained dividing them by the sampled area. The number density of each annulus was then defined as the average of the sub-sectors densities, and its standard deviation was computed from the variance among the sub-sectors.

Finally, for each system the background density contribution was estimated by using the density measurements of the outermost annuli. We notice that the background densities obtained in the outskirts of the clusters in the same field of view are consistent with each other. We then subtracted these values from the corresponding observed density profiles (see Fig. 7).

## 4.2 Best-fit dynamical models

We analyzed the number density profiles of the clusters in our sample by means of dynamical models.

We considered spherical, isotropic King (1966) models[3] and we fit them to the density profiles calculated as described in Section 4.1. We determine two fitting parameters: the structural parameter W_0, (this parameter is often referred to as concentration), and a scale radius, r_0, sometimes called King radius. A third parameter, depending on these two, is the central number density ν_0, which is needed to vertically scale the model profiles to match the observations; this parameter is related to the total number of stars belonging to the cluster.

The best-fit parameters are determined by minimizing the quantity:

$$\chi^2 = \sum_{i=1}^{N} \left[\frac{N_i - \nu_0 \, \hat{\nu}(R_i/r_0)}{\delta N_i} \right]^2 \;,$$ (1)

---

[3] To compute these models we used the code LIMEPY introduced by Gieles & Zocchi (2015), by fixing the value of the truncation parameter $g = 1$. See King (1966) and Gieles & Zocchi (2015) for more details on the models and their calculation.
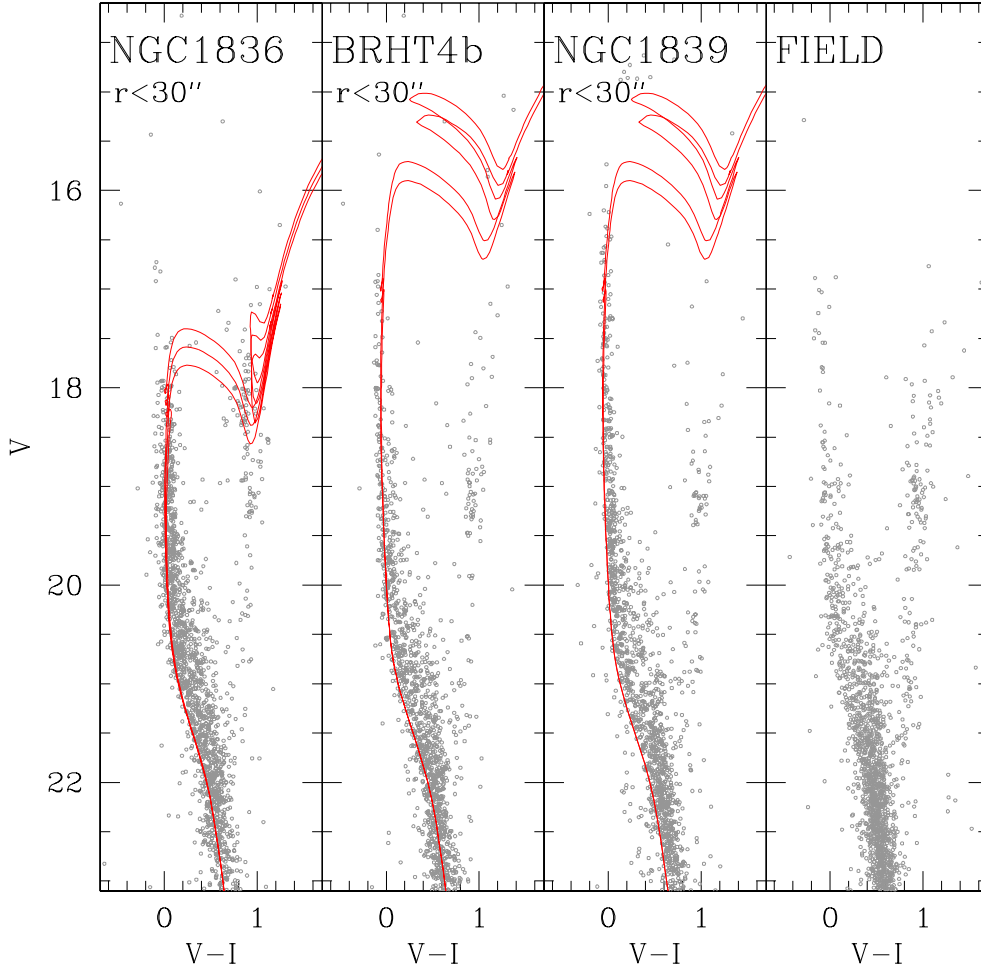
Figure 6. As in Figure 5, but for NGC1836, BRHT4b, NGC1839 and field stars. The area sampled by the field CMD is $\sim 2.1\text{arcmin}^2$.

Table 2. Best-fit parameters. For each cluster, listed in the first column, we provide the values of the best-fit parameters obtained by fitting King models to the number density profiles (see Section 4.2): the concentration parameter W_0, the King scale radius r_0 (expressed in arcsec), and the central value of the number density, ν_0 (expressed in number per arcsec^2). We also indicate the formal errors on the parameters (see Zocchi et al. 2012).

Cluster	W_0	r_0 (arcsec)	ν_0 (arcsec^{-2})
SL353	$4.78^{+1.48}_{-2.26}$	$19.36^{+6.55}_{-5.69}$	0.658 ± 0.003
SL349	$1.88^{+3.02}_{-1.73}$	$16.63^{+2.72}_{-11.37}$	0.430 ± 0.005
SL385	$5.92^{+3.94}_{-5.17}$	$8.56^{+4.60}_{-3.67}$	0.605 ± 0.009
SL387	$5.37^{+2.38}_{-4.65}$	$10.73^{+4.62}_{-5.01}$	0.634 ± 0.007
NGC1922	$6.11^{+3.02}_{-5.10}$	$7.57^{+4.47}_{-3.46}$	0.489 ± 0.008
NGC1836	$5.28^{+2.54}_{-3.72}$	$12.69^{+3.71}_{-4.80}$	0.871 ± 0.006
NGC1839	$6.20^{+0.42}_{-0.48}$	$16.01^{+4.97}_{-3.63}$	0.404 ± 0.002
BRHT4b	$5.90^{+0.70}_{-0.94}$	$12.62^{+7.78}_{-4.34}$	0.295 ± 0.003

where R_i, N_i, and δN_i are the radial position, number density and number density error for each of the N points in the number density profile of each cluster. The quantity $\hat{\nu}(R_i/r_0)$ is the projected number density of the model, normalized to its central value. The central number density ν_0 is obtained as

$$\nu_0 = \left[\sum_{i=1}^{N} \frac{N_i \, \hat{\nu}(R_i/r_0)}{\delta N_i^2} \right] \left[\sum_{i=1}^{N} \frac{\hat{\nu}(R_i/r_0)}{\delta N_i^2} \right]^{-1} , \qquad (2)$$

for each pair of values (W_0, r_0).

The best-fit parameters obtained from this fitting procedure are given in Table 2, and the best-fit profiles are shown in Fig. 7. The models appear to reproduce the observed profiles well, over their radial extent.

The profile slope in the outermost radial bins for clusters NGC1839 and BRHT4b is quite shallow. For these profiles, the models providing a good fit turn out to be extremely concentrated and tend to have as best-fitting values for W_0 and for r_0 the largest values that we explored to calculate the χ^2 function defined in equation (1) and $r_t \sim 3000''$. Thus, in order to determine the best fit, we
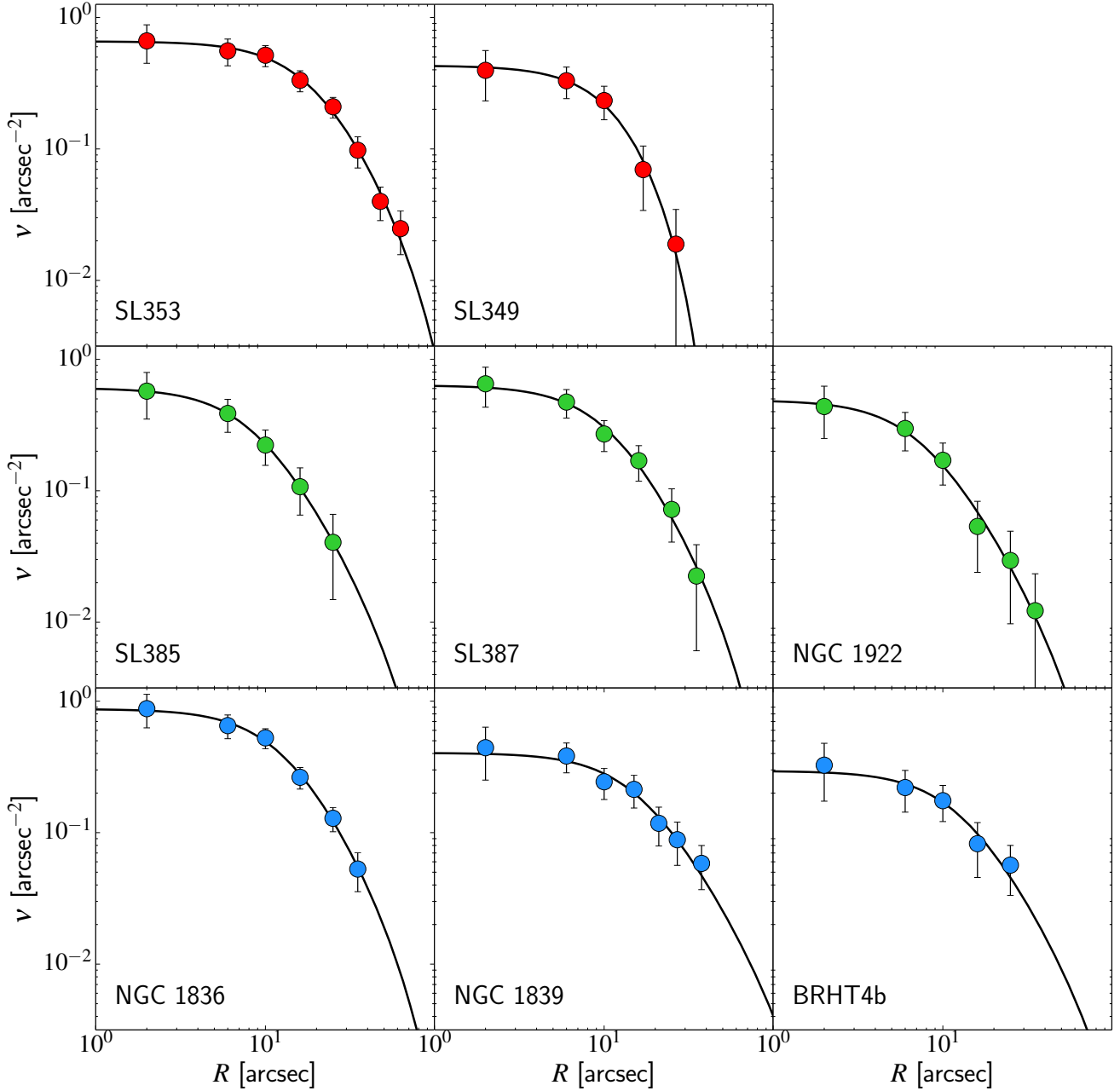
Figure 7. Number density profiles of the clusters in our sample, as indicated by the labels in the panels. Solid lines correspond to the best-fit King (1996) model fits, and the data are indicated with circles. Each row corresponds to a different group of clusters, identified also by the different colors of the points in the panels. For each data-point, vertical error bars are shown. The vertical and horizontal axes span the same range in every panel, to allow a more direct comparison among the clusters.

imposed the truncation radius r_t to be equal to r_J (see Section 5.1). This choice is a compromise between having an appropriate radial range for the density profiles of the clusters and still providing an adequate description of the data points by the models. The best-fit models of these clusters, therefore, need to be considered with caution.

5   CHARACTERIZATION OF THE CLUSTER DENSITY MAPS

5.1   Effects of the tidal environment

To understand whether these clusters are gravitationally bound and possibly tidally interacting, it is necessary to determine their Roche filling conditions. To do so, we estimated the Jacobi radius r_J of each cluster in our sample, and we compared it with the truncation radius r_t obtained

by the best-fit King models. For each cluster, the Jacobi radius may be calculated in an approximate way as:

$$r_{\rm J} = \left(\frac{GM}{\xi\,\Omega^2}\right)^{1/3} , \qquad (3)$$

where M is the mass of the cluster, G is the gravitational constant, Ω is the orbital frequency of the cluster in the LMC, and $\xi = 4 - \kappa^2/\Omega^2$, with κ the epicyclic frequency (for details see Bertin & Varri 2008). For simplicity, we describe the potential of the LMC by means of a spherical Plummer model (as done, for example, by Bekki & Chiba 2005) with scale length $b = 2.6$ kpc; such an assumption allows us to specify ξ as a simple function of the galactocentric distance R_0:
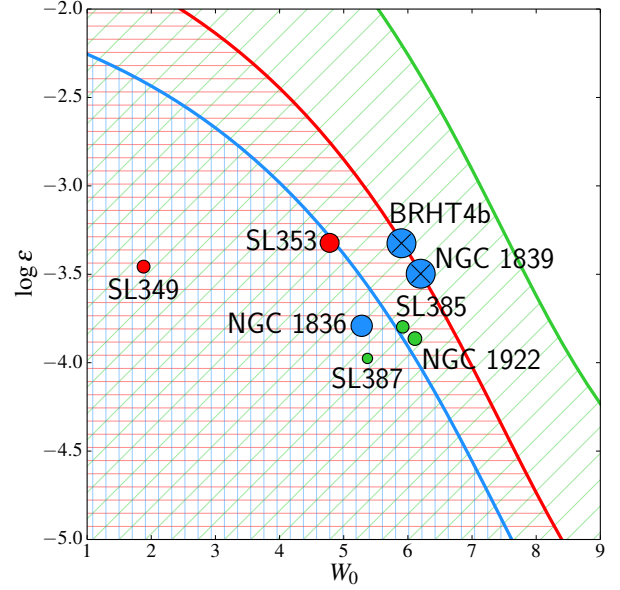
$$\xi(R_0) = \frac{3\,R_0^2}{b^2 + R_0^2} . \qquad (4)$$

To estimate the total mass of a cluster we considered the corresponding best-fit King model, and we calculated its total luminosity in V-band by opportunely scaling it to match the central surface brightness (measured directly on the images), $\mu_{\rm V,0}$. We then converted this to a mass estimate by multiplying it by the V-band mass-to-light ratio M/L appropriate for the age of the clusters and their metallicity (Maraston 1998)[4].

To calculate the value of Ω, we rely on the measures of the LMC centre and rotation curve recently obtained by van der Marel & Sahlmann (2016) as a result of their analysis of *HST* and *Gaia* proper motions (see fourth column of their Table 2). They describe the rotation curve of the LMC as a function of the distance from the centre $(\alpha_0, \delta_0 = 79.37, -69.58)$: the circular velocity increases linearly up to a velocity of 78.9 km s^{-1} at a distance of about 2.6 kpc from the centre[5], and then remains flat outwards. The clusters in our sample are in the radial range where the circular velocity is linearly increasing with the distance, therefore for all of them $\Omega = 0.03$ km s^{-1}pc^{-1}.

In Table 3 we list the values of r_J as well as the values of the quantities needed to obtain them and mentioned above. In the Table we also report the values of $r_{\rm t}/r_{\rm J}$ and $r_{\rm h}/r_{\rm J}$. These two quantities indicate the degree of filling of the Roche lobe of a given cluster. We notice that globular clusters having $r_{\rm h}/r_{\rm J} > 0.10$ are usually considered to be tidally filling (e.g., see Gieles & Baumgardt 2008; Baumgardt et al. 2010). Based on the quantities derived in Table 3 only the clusters in the NGC1836-BRHT4b-NGC1839 multiplet would be classified as tidally filling.

We further explored this aspect by considering a dimensionless quantity introduced by Bertin & Varri (2008) as one of the parameters of a family of triaxial dynamical models of stellar systems shaped by the tidal field of their hosting galaxy. This tidal strength parameter, ε, is defined as the ratio of the square of the orbital frequency of the cluster in the

---

[4] M/L values are listed at the following link http://www-astro.physics.ox.ac.uk/~maraston/SSPn/ml/ml_SSP.tab
[5] We note that we are using this value as the scale length b to describe the potential of the LMC introduced above.

Figure 8. Tidal strength parameter ε as a function of W_0. The blue, red and green lines correspond to the critical values of the tidal strength parameter, as a function of W_0, for clusters located at the galactocentric distance corresponding to parameter values $\xi = 0.01, 0.16, 0.55$ in a spherical host Plummer potential (for details, see main text). Any cluster located in the shaded region below a given line is underfilling its critical equipotential surface. The clusters in our sample are indicated with circles having the same colors used in Fig. 7 and size representing the value of their filling factor $r_{\rm t}/r_{\rm J}$. Clusters NGC1839 and BRHT4b are marked with a cross because their estimated truncation radius is chosen to be equal to their Jacobi radius.

galaxy to the square of the dynamical frequency associated with its central mass density ρ_0:

$$\varepsilon = \frac{\Omega^2}{4\pi G \rho_0} , \qquad (5)$$

where ρ_0 is here determined from the best-fit King models, and Ω is obtained as described above. We emphasize that the following analysis is aimed exclusively at the characterization of the tidal effects associated with the host galaxy, and does not account for the tidal perturbations determined by any possible gravitational interaction between the members of a cluster pair.

The two-dimensional parameter space defined by the central concentration (W_0) and the tidal strength parameter is illustrated in Fig. 8. In such a diagram, for a given choice of the galactic potential and galactocentric distance R_0, we can identify configurations corresponding to the critical values of the tidal strength parameter (marked with solid lines), as a function of the central concentration parameter (see Bertin & Varri 2008). For a given tidal environment and value of W_0, the boundary of a critical configuration is defined by the last closed equipotential surface (i.e., such that $r_{\rm t}/r_{\rm J} \approx 2/3$, for details see Varri & Bertin 2009, Sect. 2). From the bottom to the top, the lines represent the cases with $\xi = 0.01, 0.16$, and 0.55, which, for simplicity, corre-

Table 3. Relevant clusters properties. For each cluster, listed in the first column, we provide the values of several quantities: column (2) the galactocentric distance in kpc (assumed to be equal to the projected distance), (3) the truncation radius determined from the best-fit King model, expressed both in arcsec and in pc, (4) the central surface brightness in V-band, (5) the V-band mass-to-light ratio in solar units, (6) the total mass in units of 10^4 M$_\odot$, (7) the central mass density in unit of M$_\odot$ pc^{-3}, (8) the Jacobi radius, both in arcsec and in pc, (9) the logarithm of the tidal strength parameter ε, (10) the ratio of the truncation radius to the Jacobi radius, and (11) the ratio of the half-mass radius to the Jacobi radius. Quantities marked with an asterisk have been obtained by imposing, during the fitting procedure, the maximum possible value of the truncation radius (i.e., $r_t = r_j$).

(1) Cluster	(2) R_0 kpc	(3) r_t arcsec	(3) pc	(4) $\mu_{V,0}$ mag arcsec^{-2}	(5) M/L M$_\odot$/L$_\odot$	(6) M 10^4 M$_\odot$	(7) ρ_0 M$_\odot$ pc^{-3}	(8) r_J arcsec	(8) pc	(9) $\log \varepsilon$	(10) $r_\mathrm{t}/r_\mathrm{J}$	(11) $r_\mathrm{h}/r_\mathrm{J}$
SL353	0.62	186.96	45.41	19.7	0.62	4.04	35.63	434.97	105.65	-3.32	0.43	0.08
SL349	0.62	50.57	12.28	19.9	0.62	0.82	48.56	256.12	62.21	-3.46	0.20	0.06
SL385	0.15	147.16	35.74	18.4	0.26	1.57	106.38	795.17	193.14	-3.80	0.19	0.03
SL387	0.16	137.81	33.47	18.6	0.58	3.86	160.50	1027.33	249.53	-3.98	0.13	0.02
NGC1922	0.19	145.04	35.23	17.9	0.17	1.35	123.96	645.27	156.73	-3.86	0.22	0.03
NGC1836	1.25	155.13	37.68	18.4	0.37	3.99	104.94	285.68	69.39	-3.79	0.54	0.10
NGC1839	1.22	323.75*	78.64*	18.0	0.17	5.70	53.26	323.75	78.64	-3.50	1.00*	0.14
BRHT4b	1.24	214.50*	52.10*	18.7	0.17	1.68	35.82	214.50	52.10	-3.32	1.00*	0.15

sponds to the numerical average of the individual values of the parameter ξ (see equation 4) resulting from the values of the galactocentric radii of the multiplets members (see Table 3, Col. 2). The hatched regions indicate configurations that are tidally underfilling, and, moving from the critical lines towards the bottom left corner of the parameter space, that are progressively less affected by the tidal perturbation. The clusters in our sample are indicated in the figure with circles of variable sizes; their diameter represents the value of their filling factor $r_\mathrm{t}/r_\mathrm{J}$. Clusters NGC1839 and BRHT4b are marked with a cross because their estimated truncation radius is chosen to be equal to their Jacobi radius (i.e., they correspond to overcritical configurations). The circles and their corresponding critical lines have the same colors used in Fig. 7. A better estimate of the LMC potential would provide a more accurate estimate of the tidal radii and of the tidal strength of these clusters.

Clusters SL349 and SL353 (indicated with red circles in the figure) have similar tidal strength but very different concentration; the first one, which is less massive and strongly underfilling, is well within the region indicating model tidal interactions, while SL353 is relatively close to the condition of critical filling; in our sample, this pair is indeed characterized by the largest distance between members ($\sim$ 18 pc). Clusters SL387 and SL385 (green circles in the figure) are located at a relative distance of $\approx$ 11pc and they are both tidally underfilling (i.e., fall below the critical green line). Finally, NGC1836 and BRHT4b (blue circles in the figure), which are at a relative distance of $\sim$ 10 pc, have a very similar concentration but different tidal strengths, with the first being underfilling and the second being overfilling. It is important to clarify that BRHT4b and NGC1839 are overfilling by construction as we fixed $r_\mathrm{t} = r_J$. Also, it is worth noting that NGC1836 is almost critically filling its Roche lobe (as illustrated by its proximity to the critical blue line).

This analysis confirms that virtually all clusters in our sample are tidally underfilling. We also note that for all the clusters (except NGC1839 and BRHT4b, for which we do not have a reliable estimate for the truncation radius and

we fixed it to be $r_\mathrm{t} = r_\mathrm{J}$), the Jacobi radius results to be larger than the truncation radius. For all candidate binary clusters, both the truncation radius and the Jacobi radius are estimated to be larger than the distance between them with the only exception being SL349, which has a very small truncation radius ($r_\mathrm{t} = 12.28$ pc).

In such a configuration, and assuming that the projected distances are compatible with the real ones, the presence of intra-clusters stellar streams or bridges would be a strong indication that they are gravitationally bound as each one would fall within the Roche lobe (and in some cases even within the spatial truncation) of the companion. Very interesting are also the cases of SL353 and NGC1836, which are approaching conditions of critical filling, and therefore they are likely starting to loose stars trough their Roche lobes.

5.2   Characterization of the intra-cluster over-densities

To probe the spatial distribution of cluster pairs and the possible presence of interaction signatures, we analyzed their 2D density distributions. The density analysis has been performed in the entire FORS2 FOV for each multiplet using only stars with $V \leq 21$ in order to limit the impact of the background. The distribution of star positions was transformed into a smoothed surface density function through the use of a kernel whose width has been fixed at $10''$ (see Dalessandro et al. 2015b). This procedure yields the surface density distribution shown as an example in Figure 9 (left panel) for SL349-SL353. Each cluster appears to be quite spherical and a significant overdensity (a sort of bridge) between the two is clearly observed. This result is qualitatively compatible to what was found by Dieball et al. (2000), however we do not confirm the elongation the authors observed in SL353. We argue that such a discrepancy is likely due to the use of shallow photometry by (Dieball et al. 2000), which might be prone to low-number statistics and fluctuations in the distribution of bright stars.

In general, we find that all cluster pairs in our sample
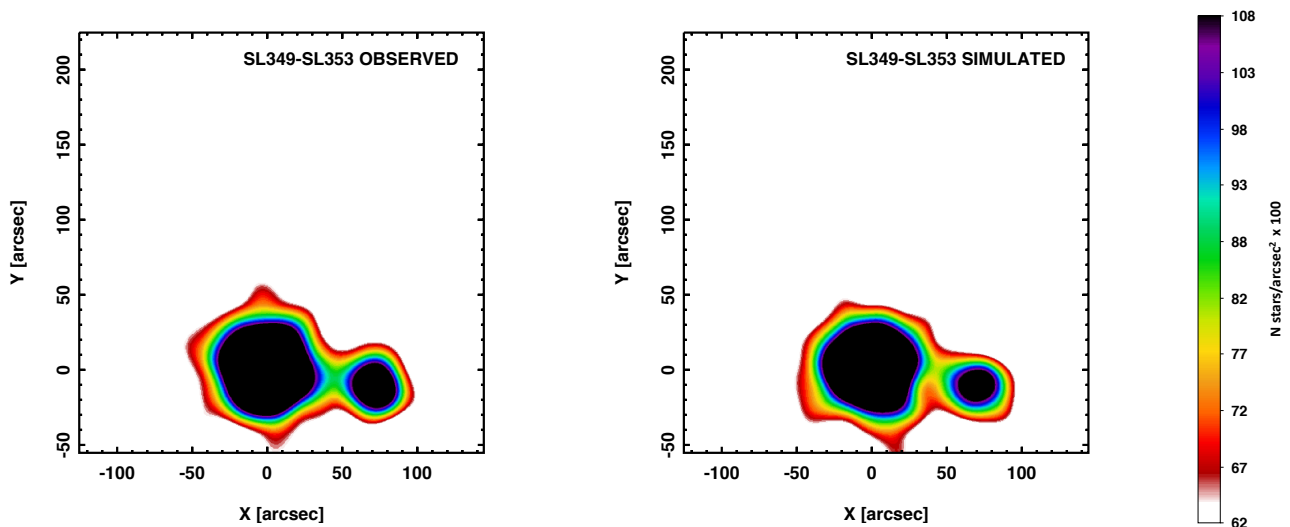
Figure 9. Number density map for the clusters SL353 and SL349. The left panel shows the density map measured from the observations, the right panel the density map obtained from one of our 1000 simulated samples to reproduce this cluster pair. The color code presented in the bar on the right indicates the density scale.

show evidence of intra-cluster overdensities. These features could be an indication of an ongoing interaction between the clusters and therefore of their binarity. On the other hand however, they could be also due to projection effects.

In order to constrain the nature of the observed intra-cluster overdensities, we used the best-fit King models described above. For each pair of clusters, we generated 1000 simulated observations by sampling the distribution function of its best-fitting King model to randomly generate a set of stars. We locate the clusters at their relative positions, and we also simulated a uniform background, by using the background density we measured and subtracted from the number density profiles (see Section 4.1). For each cluster, we used the value of the parameter ν_0 obtained from the fitting procedure to scale the best-fit model density profiles: this allows us to obtain an estimate of the total number of stars observed in each cluster (by integrating the number density over the area). We then use this number to set the amount of stars to simulate in order to reproduce each cluster. After simulating each candidate cluster pair, we checked that the total number of stars in the clusters and the background are consistent with the total number of observed stars. Figure 9 provides a comparison between the measured number density map in the field of view of SL349 - SL353 and the same map obtained by considering one of the simulated observations. The two panels show qualitatively similar density maps and in particular we observe that intra-cluster overdensities are clearly detectable also in our simulations.

To provide a more quantitative comparison, for each simulated configuration we selected a rectangular region connecting the two candidate binary clusters, with length equal to the distance between their centers and width of 10 arcsec. We divided this region into equal size bins and we calculated the number density of stars in each bin. Then, we computed the quantiles of the distribution in each bin, to obtain the median and the 1σ, 2σ and 3σ values for each bin. Figures 10, 11, and 12 show the result for the three candidate

binary clusters. The thick solid line represents the median of the distribution of the number density, the shaded areas correspond to 1σ, 2σ and 3σ from the median. The dashed line indicates the uniform density that we assumed for the background. The black points, with their vertical error bars, represent the number density measured in the corresponding bins in the observed distribution.

The comparison between the observations and the simulations would suggest that the overdensity between clusters in the candidate pairs is consistent with them being close to each other in projection. We do not observe any additional feature indicating ongoing strong tidal interactions between the members of the pairs.

6 DISCUSSION AND CONCLUSIONS

We presented a detailed photometric analysis of three candidate cluster pairs in the LMC with the aim of characterizing their properties and constraining their possible binarity. Specifically, we have derived their ages, determined their structural and morphological properties and investigated the possible presence of signatures of gravitational interactions between the members of a given pair.

We found that the members of the pair SL349 - SL353 share the same age ($t = 1.00 \pm 0.12$ Gyr), thus suggesting that these systems possibly formed from the fragmentation of the same molecular cloud. Also BRHT4b and NGC1839 have similar ages ($t = 140 \pm 15$ Myr). Given their projected distance however, it is unlikely that these systems form a true pair, while of course we cannot exclude they have a common origin. SL385, SL387 and NGC1922 show significant age differences and therefore they likely formed in different clouds.

By means of simple, single-mass, isotropic King (1966) models, we have derived an estimate of the structural parameters of all star clusters in our sample. In addition, we have also provided an approximate estimate of the critical
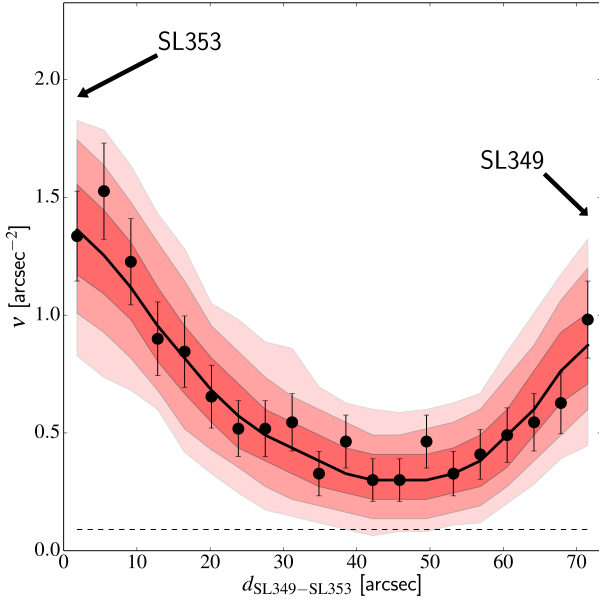
Figure 10. Black points with vertical error bars indicate the number density measured from the data along the line connecting clusters SL353 and SL349 on the plane of the sky. The thick solid line represents the median of the distribution of the number density calculated from the 1000 random realization of the simulated observations in the same sky region, the shaded areas correspond to 1σ, 2σ and 3σ from the median. The dashed line indicates the uniform background density.
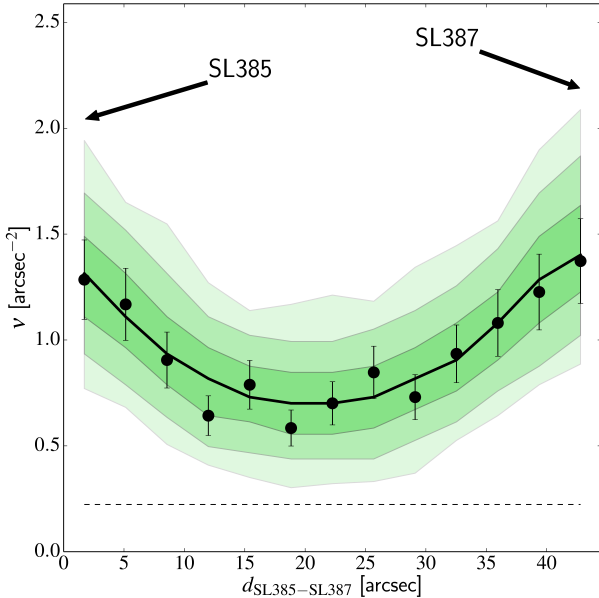
Figure 11. Same as Fig. 10, but for SL385 and SL387.
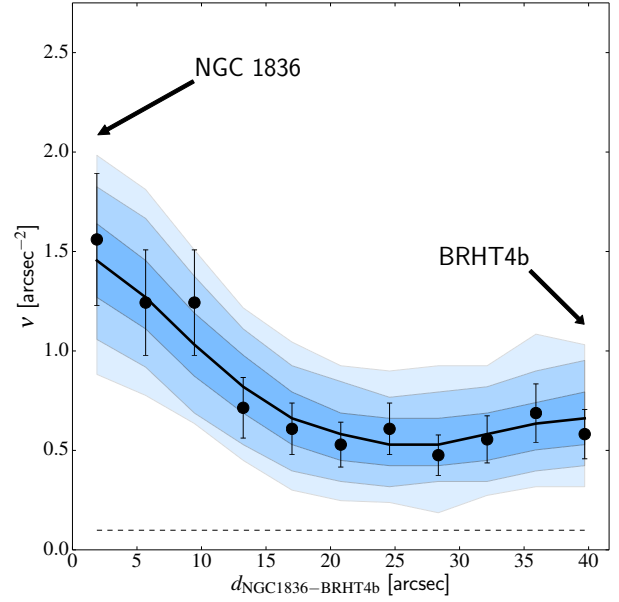
Figure 12. Number density along the line connecting clusters NGC1836 and BRHT4b on the plane of the sky. The format of this figure is the same as Fig. 10.

equipotential surface and Jacobi (tidal) radius of the star clusters, as a zeroth-order tool to evaluate the extension of their Roche lobe, as determined by the interaction with the tidal field of the LMC. We wish to emphasize that our study has a number of limitations. First of all, our simple dynamical analysis is based exclusively on the interpretation of photometric data, which do offer only a very partial, and often degenerate, view of the internal properties of star clusters (e.g., see Zocchi et al. 2012, 2016). Second, the methodology for the calculation of both the truncation and tidal radius of the clusters in our study do not take into account the effects of possible gravitational interactions between the members of a given pair. Third, the calculation of the Jacobi radius of the clusters in our sample is also based on a relatively crude estimate of their orbital frequencies which, in turn, relies on a particularly simplified description of the potential of the LMC and on the heavy assumption that the three-dimensional galactocentric distance of the clusters correspond to the distance in projection.

None the less, the simple structural information we have determined for the clusters in our sample have allowed us to evaluate their degree of filling, therefore, to have a first assessment of the strength of the perturbation associated with the external tidal field. All clusters appear to be underfilling their Roche lobe, with NGC1836 and SL353 being relatively close to the condition of critical filling (see Table 3 and Fig. 9). For all candidate binary clusters, both the truncation radius and the Jacobi radius are estimated to be larger than the distance between them. In such a configuration, and assuming that the projected distances are compatible with the real ones, the presence of intra-clusters stellar streams or bridges would be a strong indication that they are gravitationally bound as each one would fall within

the Roche lobe (and in some cases even within the spatial truncation) of the companion.

Indeed all clusters show evidence of intra-cluster overdensities. However, it appears to be impossible with basically only photometric information to distinguish the case in which there is a genuine presence of ongoing mass-transfer from the case in which the members are simply sufficiently close to each other so that the tenuous mass distribution in their outer regions appears, in projection, to be a joined mass distribution.

Among the candidate cluster pairs, the case of SL349 - SL353 is particularly interesting. In fact, Dieball et al. (2000) measured the radial velocities of a sample of individual stars in both systems. While the sample of member stars is small (4 and 5 for SL349 and SL353 respectively), the authors concluded that the clusters have very similar mean velocities ($v_{SL349} \sim 274 \pm 10$ km s^{-1} and $v_{SL353} \sim 279 \pm 4$ km s^{-1}) and they could share a common center of mass.

All these elements, coupled with the fact that SL349 and SL353 share the same age ($t \sim 1$ Gyr) contribute to form a dynamical interpretation according to which the clusters SL349 and SL353 might actually be the members of an energetically bound pair. It is therefore imperative to pursue a more detailed kinematical analysis of such clusters, without which, at present, we do not dare making a conclusive statement about the true nature of this pair. Such a degeneracy in the interpretation may be broken exclusively by coupling the currently available photometric information with an appropriate kinematical characterization covering the entire radial extension of the clusters, and, ideally, of any star in the intra-cluster region.

ACKNOWLEDGEMENTS

REFERENCES

Amaro-Seoane, P., Konstantinidis, S., Brem, P., & Catelan, M. 2013, MNRAS, 435, 809
Arnold, B., Goodwin, S. P., Griffiths, D. W., & Parker, R. J. 2017, MNRAS, 471, 2498
Barnes, J., & Hut, P. 1986, Nature, 324, 446
Baumgardt, H., Makino, J., Hut, P., McMillan, S., & Portegies Zwart, S. 2003, ApJl, 589, L25
Baumgardt, H., Parmentier, G., Gieles, M., & Vesperini, E. 2010, MNRAS, 401, 1832
Bekki, K., Beasley, M. A., Forbes, D. A., & Couch, W. J. 2004, ApJ, 602, 730
Bekki, K., & Chiba, M. 2005, MNRAS, 356, 680
Bertin, G., & Varri, A. L. 2008, ApJ, 689, 1005-1019
Bhatia, R. K., & Hatzidimitriou, D. 1988, MNRAS, 230, 215
Bhatia, R. K. 1990, PASJ, 42, 757
Bhatia, R. K., Read, M. A., Hatzidimitriou, D., & Tritton, S. 1991, A&AS, 87, 335
Bica, E., Claria, J. J., Dottori, H., Santos, J. F. C., Jr., & Piatti, A. E. 1996, ApJS, 102, 57
Bressan, A., Marigo, P., Girardi, L., et al. 2012, MNRAS, 427, 127

Brüns, R. C., & Kroupa, P. 2011, ApJ, 729, 69
Catelan, M. 1997, ApJl, 478, L99
Dalessandro, E., Ferraro, F. R., Massari, D., et al. 2015, ApJ, 810, 40
Dalessandro, E., Miocchi, P., Carraro, G., Jílková, L., & Moitinho, A. 2015, MNRAS, 449, 1811
Dalessandro, E., Ferraro, F. R., Massari, D., et al. 2013, ApJ, 778, 135
de La Fuente Marcos, R., & de La Fuente Marcos, C. 2009, A&A, 500, L13
de Oliveira, M. R., Bica, E., & Dottori, H. 2000, MNRAS, 311, 589
De Silva, G. M., Carraro, G., D'Orazi, V., et al. 2015, MNRAS, 453, 106
Dieball, A., Grebel, E. K., & Theis, C. 2000, A&A, 358, 144
Dieball, A., Müller, H., & Grebel, E. K. 2002, A&A, 391, 547
Efremov, Y. N. 1995, AJ, 110, 2757
Elmegreen, B. G., & Elmegreen, D. M. 1983, MNRAS, 203, 31
Gardiner, L. T., & Noguchi, M. 1996, Journal of Korean Astronomical Society Supplement, 29, S93
Goodwin, S. P., & Whitworth, A. P. 2004, A&A, 413, 929
Fall, S. M., Chandar, R., & Whitmore, B. C. 2005, ApJL, 631, L133
Gavagnin, E., Mapelli, M., & Lake, G. 2016, MNRAS, 461, 1276
Gieles, M., & Baumgardt, H. 2008, MNRAS, 389, L28
Gieles, M., & Zocchi, A. 2015, MNRAS, 454, 576
Girardi, L., Chiosi, C., Bertelli, G., & Bressan, A. 1995, A&A, 298, 87
Haschke, R., Grebel, E. K., & Duffau, S. 2011, AJ, 141, 158
Hatzidimitriou, D., & Bhatia, R. K. 1990, A&A, 230, 11
Holland, S., Fahlman, G. G., & Richer, H. B. 1995, AJ, 109, 2061
Hong, J., de Grijs, R., Askar, A., et al. 2017, MNRAS, 472, 67
Inno, L., Bono, G., Matsunaga, N., et al. 2016, ApJ, 832, 176
Kallivayalil, N., van der Marel, R. P., Besla, G., Anderson, J., & Alcock, C. 2013, ApJ, 764, 161
King, I. R. 1966, AJ, 71, 64
Kumai, Y., Basu, B., & Fujimoto, M. 1993, ApJ, 404, 144
Lanzoni, B., Dalessandro, E., Ferraro, F. R., et al. 2007, ApJl, 668, L139
Larsen, S. S. 2000, MNRAS, 319, 893
Lee, Y.-W., Joo, J.-M., Sohn, Y.-J., et al. 1999, Nature, 402, 55
Leon, S., Bergond, G., & Vallenari, A. 1999, A&A, 344, 450
Makino, J., Akiyama, K., & Sugimoto, D. 1991, Ap&SS, 185, 63
Maraston, C. 1998, MNRAS, 300, 872
Minniti, D., Rejkuba, M., Funes, J. G., & Kennicutt, R. C., Jr. 2004, ApJ, 612, 215
Mucciarelli, A., Carretta, E., Origlia, L., & Ferraro, F. R. 2008, AJ, 136, 375
Mucciarelli, A., Origlia, L., Ferraro, F. R., Bellazzini, M., & Lanzoni, B. 2012, ApJl, 746, L19
Okumura, S. K., Ebisuzaki, T., & Makino, J. 1991, PASJ, 43, 781
de Oliveira, M. R., Dottori, H., & Bica, E. 1998, MNRAS, 295, 921
Piatti, A. E., de Grijs, R., Ripepi, V., et al. 2015, MNRAS, 454, 839
Portegies Zwart, S. F., & Rusli, S. P. 2007, MNRAS, 374, 931
Priyatikanto, R., Kouwenhoven, M. B. N., Arifyanto, M. I., Wulandari, H. R. T., & Siregar, S. 2016, MNRAS, 457, 1339
Stetson, P. B. 1987, PASP, 99, 191
Stetson, P. B. 1994, PASP, 106, 250
Subramaniam, A., Gorti, U., Sagar, R., & Bhatt, H. C. 1995, A&A 302, 86
Sugimoto, D., & Makino, J. 1989, PASJ, 41, 1117
Surdin, V. G. 1991, Ap&SS, 183, 129
Vallenari, A., Bettoni, D., & Chiosi, C. 1998, A&A, 331, 506
van den Bergh, S. 1996, ApJl, 471, L31
van der Marel, R. P., & Sahlmann, J. 2016, ApJl, 832, L23
Varri, A. L., & Bertin, G. 2009, ApJ, 703, 1911

Zaritsky, D., Harris, J., Thompson, I. B., & Grebel, E. K. 2004, AJ, 128, 1606

Zocchi, A., Bertin, G., & Varri, A. L. 2012, A&A, 539, A65

Zocchi, A., Gieles, M., Hénault-Brunet, V., & Varri, A. L. 2016, MNRAS, 462, 696

This paper has been typeset from a TeX/LaTeX file prepared by the author.